Bone mesenchymal stem cell-derived exosome-encapsulated microRNA-125b-5p inhibits ovarian cancer progression via DDX5 downregulation

YUXIA WANG[1*], WEI WANG[1*], DAN ZHENG[2] and YING GAO[1]

[1]Department of Gynecology, Harbin Medical University Cancer Hospital, Harbin, Heilongjiang 150081, P.R. China;
[2]Department of Gynecology, Harbin Red Cross Central Hospital, Harbin, Heilongjiang 150076, P.R. China

Received May 21, 2024; Accepted November 7, 2024

DOI: 10.3892/ol.2025.15001

Abstract. Exosomes can be used to mediate the delivery of nucleic acids such as microRNA-125b-5p (miR-125b-5p), a tumor-suppressor in certain types of cancer, into tumor cells. The present study investigated the use of bone mesenchymal stem cells-derived exosome (BMSCs-Exo) delivery of miR-125b-5p in ovarian cancer (OC). BMSCs were transfected with miR-125b-5p mimic, from which exosomes termed Exo-miR-125b-5p mimic were extracted. The expression levels of miR-125b-5p in OC tissue samples, BMSCs, exosomes and SKOV3 cells were quantified using reverse transcription-quantitative PCR. The influence of Exo-miR-125b-5p mimic on the biological functions of OC was evaluated through cell proliferation, invasion, migration and apoptosis assays. The targeting relationship between miR-125b-5p and DEAD-box helicase 5 (DDX5) was verified, and the expression levels of DDX5 in OC samples and SKOV3 cells were quantified using western blotting. miR-125b-5p was downregulated in tumor tissue samples from patients with OC. BMSCs-Exo reduced the malignant properties of SKOV3 cells *in vitro*, and these effects were be advanced by miR-125b-5p upregulation. miR-125b-5p targeted and inhibited DDX5 expression. DDX5 overexpression inhibited Exo-miR-125b-5p-induced suppression of OC development. Overall, this study highlights that BMSCs-Exo-encapsulated miR-125b-5p inhibited OC progression via DDX5 downregulation, providing insight into the molecular mechanisms underlying OC.

Correspondence to: Dr Ying Gao, Department of Gynecology, Harbin Medical University Cancer Hospital, 150 Haping Road, Nangang, Harbin, Heilongjiang 150081, P.R. China
E-mail: gaoying8007@163.com

*Contributed equally

Key words: ovarian cancer, bone mesenchymal stem cells, exosomes, microRNA-125b-5p, DEAD-box helicase 5, tumor

Introduction

Ovarian cancer (OC) was the eighth most commonly diagnosed malignancy in the Global Cancer Statistics 2020 (1), with an estimated age-standardized incidence rate of 6.6%. OC can be classified into three main types: i) Epithelial OC (EOC); ii) sex cord stromal OC; and iii) germ cell OC, the latter two accounting for ~5% of all OC cases (2). The main symptoms of OC are persistent abdominal pain, abdominal distension or bloating, urinary system symptoms, frequent urination and non-specific gastrointestinal symptoms (3). After primary debulking surgery, intravenous or intraperitoneal chemotherapy is preferentially administrated to eliminate cancer cells and maintenance drugs, such as olaparib and bevacizumab, are used to slow recurrence (4). The identification of complete molecular mechanisms underlying OC is required to more efficiently prevent and treat OC.

Mesenchymal stem cells (MSCs) are pluripotent stromal cells with multiple differentiation capabilities, and bone marrow is a typical source of MSCs (5). In addition to MSCs, their nanoghosts (nanovesicles reconstructed from the cytoplasmic membranes of MSCs) also have promising therapeutic effects on certain types of cancer, including gastrointestinal, lung and ovarian cancer (6). MSCs may secret large amounts of exosomes (Exos) for cell-to-cell communication and keep a dynamic and homeostatic microenvironment for tissue repair. The use of MSCs-derived exosomes (MSCs-Exo) may have notable advantages over their living cells and may reduce adverse side effects (7). MSCs-Exo possess numerous advantages, consisting of non-immunogenicity, easy accessibility for isolation and preparation, convenient storage at low temperature, non-infusion toxicity and freedom from tumorigenic potential and ethical issues (8). MSCs-Exo have pluripotent functions through delivery of targeted microRNAs (miRs/miRNAs) in certain types of human cancer (for example ovarian, breast and prostate cancer), including increasing drug sensitivity (9), promoting dormancy (10) and restraining tumorigenesis (11).

Recognition of miRNA signatures has identified miR-125b-5p as a biomarker of endometrial cancer (12). In fact, miR-125b-5p downregulation is indicative of poor prognosis in EOC (13) whereas miR-125b-5p upregulation

inhibits tumor growth in combination with cisplatin in a mouse model with OC (14). DEAD-box helicase 5 (DDX5) is an active RNA helicase that is involved in cancer progression when it is upregulated by altering transcription and signaling pathways (for example, the Wnt/β-catenin-ferroptosis axis and the mTOR signaling pathway) (15-17). Expression levels of DDX5 are associated with platinum resistance in OC (18), but regulation of DDX5 can mediate the malignant phenotype of tumor cells (17,19). In the present study, a targeting relationship between miR-125b-5p and DDX5 was hypothesized using bioinformatical analysis via the online ENCORI database, therefore, the aim of the study was to investigate whether BMSCs-Exo delivery of miR-125b-5p could impede the progression of OC through modulation of DDX5 expression levels.

Materials and methods

Ethical approval. Experiments were performed following approval from the Ethics Committee of Harbin Medical University Cancer Hospital (approval no. 20200316; Harbin, China), and written informed consent from each patient was obtained. Bone MSCs (BMSCs) were used in accordance with the International Society for Stem Cells Research guidelines for Stem Cell Research and Clinical Translation and approved by the Ethics Committee of Harbin Medical University Cancer Hospital (approval no. 20200518).

Clinical subjects. The present study included 100 patients with ovarian cancer who underwent surgical treatment in the Department of Gynecology of Harbin Medical University Cancer Hospital (Heilongjiang, China) from May 2020 to January 2023, and these patients were aged 39-67 years, with an average age of 55.31±7.64 years. Inclusion criteria: i) Patients were diagnosed with ovarian cancer through pathological diagnosis; ii) no chemotherapy, radiotherapy or other treatments were performed before surgery; iii) the patients' ages were ≥18 years old; and iv) patients had complete medical records. Exclusion criteria: i) Patients had with other malignant tumors; and ii) patients with an expected survival period of no more than 3 months. Ovarian cancer tissue and normal tissue adjacent to the cancer (distance >3 cm from the cancer tissue) were collected, and biological biopsy was performed on the normal tissue adjacent to the cancer to confirm the absence of cancer cells. The tissue samples (~1 mm^3) were first rapidly frozen in liquid nitrogen for 30-60 sec, then stored in a -80˚C freezer for later use. All samples were diagnosed with ovarian cancer by pathologists who did not participate in this study.

Bone marrow specimens were also collected from 3 patients (2 males and 1 female) who received inpatient treatment in the Harbin Medical University Cancer Hospital for femoral head necrosis during May 2020 to January 2023, aged 20-55 years old. Inclusion criteria for patients: Aged >18 years old; without high femoral head drop or trauma; no cardiovascular disease or malignant tumors; and all underwent hip arthroplasty. Exclusion criteria for patients: Presence of hematological diseases; severe liver or kidney dysfunction; history of smoking; and a history of alcohol consumption. During surgery, after the femoral head was excised and the femoral medullary cavity was reamed, fresh bone marrow (5-7 ml) was collected and placed into a 10 ml sterile syringe preloaded with sodium heparin. Subsequently, the bone marrow sample was transferred to a 15 ml sterile centrifuge tube and immediately used for BMSCs isolation.

Cell culture. DMEM (Sigma-Aldrich; Merck KGaA) containing 10% FBS (Biological Industries; Sartorius AG), 100 U/ml penicillin and 100 mg/ml streptomycin (Gibco; Thermo Fisher Scientific, Inc.) was used to culture the OC cell line SKOV3 (American Type Culture Collection), and incubated in a 95% humidified atmosphere at 37˚C with 5% CO_2. The medium was replaced once every 2 days (20).

Separation and identification of BMSCs. BMSCs were isolated from bone marrow samples as previously reported (21). In brief, BMSCs were isolated by a density gradient centrifugation, followed by suspension in α-MEM supplemented with 20% FBS, 1% L-glutamine (Invitrogen (21); Thermo Fisher Scientific, Inc.) and 1% penicillin/streptomycin. The cells were then plated at a density of $1x10^6$ cells/cm^2. The culture medium was replaced after 4 days, with the non-adherent cells removed by PBS washing and the adherent cells were then cultured to reach 70-80% confluence. After that, the cells were sub-cultured in low-glucose DMEM (DMEM-LG) with the aforementioned supplements. BMSCs at passages 3 or 4 were chosen for subsequent studies.

Following this, adipogenesis was induced for 21 days in cultures by addition of DMEM-LG containing hydrocortisone (0.5 μM), 10% FBS, oboutyl methyl xanthine (0.5 μM), insulin (10 μg/ml) and indomethacin (60 μM). The medium was replaced 3 times a week. Lipid droplet formation was induced for 21 days in cultures and detected using Oil Red Osteogenic (Oil Red O; Sigma-Aldrich; Merck KGaA), followed by 1 h Oil Red O staining at room temperature. Through the addition of DMEM-LG containing 10% FBS, ascorbic acid ($2.0x10^{-4}$ mol/l), dexamethasone ($1.0x10^{-8}$ mol/l), β-glycero-phosphate ($7x10^{-3}$ mol/l), β-glycero-phosphate (10 μmol/l), dexamethasone (0.1 μmol/l) and ascorbate (50 μmol/l). The cell cultures were stained with Alizarin Red S (Sigma-Aldrich; Merck KGaA) for 5 min at room temperature to assess mineralization.

BMSCs were subjected to dissociation using trypsin/EDTA (Thermo Fisher Scientific, Inc.), cells were blocked with 3% BSA (Gibco; Thermo Fisher Scientific, Inc.) for 30 min at room temperature and the cell suspensions were dyed using multiple antibodies against MSC markers at room temperature for 30 min, consisting of CD29-FITC (1:100; cat. no. 561796), CD90-FITC (1:100; cat. no. 561969), CD44-FITC (1:100; cat. no. 561859) and CD45-FITC (1:100; cat. no. 561867) (BD Biosciences) and HRP-labeled secondary goat anti-mouse IgG antibody (1:100; cat. no. 555988) (BD Biosciences). In addition, the cells were marked with isotype-matched antibodies, which served as background controls. After the cells were treated with the appropriate secondary antibodies, followed by sample analysis using the FACSCalibur™ cytometer (BD Biosciences). Data were analyzed using the CellQuest™ pro software (version 5.1; BD Biosciences).

Isolation and purification of exosomes. BMSCs were rinsed with PBS and then moved to a conditioned medium (DMEM)

containing exosome-depleted FBS obtained by centrifugation at 120,000 x g and 4˚C for 18 h. FBS was centrifuged at 120,000 x g and 4˚C for 18 h to remove exosomes and then used to culture BMSCs. After 48 h, cells or cellular debris were removed by centrifugation at 800 x g for 10 min at 4˚C, and the supernatant was obtained and then centrifuged again (5,000 x g, 4˚C, 10 min) to ensure that all cells or cellular debris were removed to obtain the culture supernatant.

Ultracentrifugation was used for the extraction of exosomes. In detail, the live cells were removed through centrifugation at 300 x g for 10 min, the dead cells were removed at 2,000 x g for 10 min, followed by removing cell debris at 10,000 x g for 30 min and lastly, at 110,000 x g for 70 min. The aforementioned centrifugation steps were performed at 4˚C. Subsequently, the supernatant was removed to acquire exosome pellets. The exosomes were filtered using a 0.22-μm filter after PBS washing, which were then centrifuged at 110,000 x g 4˚C for 70 min. Afterward, exosomes were resuspended in PBS and maintained at -80˚C for future use. BMSCs were transfected with either 10 nM miR-125b-5p mimic or 10 nM scrambled miRNA (a negative control of miR-125b-5p mimic; mimic NC) using Lipofectamine® 3000 (Invitrogen; Thermo Fisher Scientific, Inc.) at 37˚C (the sequences are presented in Table SI). Upon 48 h transfection, the culture medium was harvested to extract exosomes, which were termed Exo-miR-125b-5p mimic and Exo-mimic NC. The secreted number of exosomes was quantified using a BCA protein assay kit (Thermo Fisher Scientific, Inc.) (22).

Characterization and quantification of exosomes. The harvested exosomes were loaded on to 400 mesh carbon grids and then fixed with 2.5% glutaraldehyde at 4˚C for 5 min and dyed using 2.5% uranyl acetate at room temperature for 10 min (Electron Microscopy Sciences) and embedded with 1% methyl cellulose on ice for 10 min (MilliporeSigma). Next, the grid was dried completely at room temperature. Transmission electron microscopy (TEM; JEM-2100F; JEOL, Ltd.) was performed to characterize the exosome's morphology. The size distribution and concentration of exosomes were analyzed by nanoparticle-tracking analysis with a NanoSight NS300 instrument (Malvern Panalytical, Malvern, UK) following the manufacturer's instructions. The expression levels of exosome proteins CD9 and CD81 were evaluated by western blotting.

Exosome uptake assay. Exosomes were fluorescently labeled with PKH26 (Sigma-Aldrich; Merck KGaA) following the manufacturer's instructions. PKH26-labeled exosomes (50 μg) incubated for 24 h with SKOV3 cells at 37˚C. Aliquots of the cell suspension were placed on microscope slides and subsequently mounted by a coverslip with the Aqua-Poly/Mount (Polysciences, Inc.). After that, nuclei were labelled blue using DAPI at 37˚C for 10 min. Images of the exosomes' cellular uptake was captured with a confocal laser scanning microscope (Carl Zeiss AG) (23).

Cell grouping and treatment. To evaluate the influence of BMSCs-derived exosomes (BMSCs-Exo) carrying miR-125b-5p targeting DDX5 on the biological functions of SKOV3 cells, the following groups were evaluated: i) Control (PBS co-cultured with SKOV3 cells); ii) Exo (BMSCs-Exo co-cultured with SKOV3 cells); iii) Exo-mimic NC (Exo-mimic NC co-cultured with SKOV3 cells); iv) Exo-miR-125b-5p mimic (Exo-miR-125b-5p mimic co-cultured with SKOV3 cells); v) small interfering RNA (siRNA)-NC (si-NC transfected into SKOV3 cells); vi) si-DDX5 (DDX5 siRNA transfected into SKOV3 cells); vii) Exo-miR-125b-5p mimic + pcDNA-NC (Exo-miR-125b-5p mimic was co-cultured with SKOV3 cells and transfected using the pcDNA3.1 plasmid); and viii) Exo-miR-125b-5p mimic + pcDNA-DDX5 (Exo-miR-125b-5p mimic was co-cultured with SKOV3 cells and transfected with pcDNA3.1 plasmid over-expressing DDX5) groups. The corresponding exosomes (50 μg) were co-incubated with SKOV3 cells ($1x10^6$ cells/well) for 24 h, respectively. The si-DDX5, si-NC, pcDNA-DDX5 and pcDNA-NC were transfected into SKOV3 cells using Lipofectamine® 3000. The aforementioned vectors and plasmids used for transfection were purchased from Shanghai GenePharma Co., Ltd., and the miR-125b-5p mimic (cat. no. MC10148) and mimic NC (cat. no. 4464059) were purchased from Thermo Fisher Scientific, Inc. (Table SI).

Cell counting kit (CCK-8) assay. SKOV3 cells were seeded at 2,000 cells/well in 96-well plates. After incubation with 10 μl CCK-8 reagent (Dojindo Laboratories, Inc.) for 2 h at 37˚C, absorbance at 450 nm was read using a SpectraMax™ 190 spectrophotometer plate reader (24).

Scratch assay. The 90% confluent, serum-starved SKOV3 cells were seeded into 6-well plates (50,000 cells/well) for 24 h and then scratched using a 200 μl pipette tip. At 0 and 48 h, images of the cells were captured using an optical microscope and wound healing rate was calculated as previously described (25).

Transwell assay. SKOV3 cells ($5x10^5$ cells/ml) were resuspended in FBS-free medium. The Matrigel-coated (coat at 4˚C, then allow gelation for 2-3 h) upper chamber of 24-well inserts Transwell plate (pore size, 8 μm; Corning, Inc.) was covered with cell resuspension (100 μl) and the lower chamber with DMEM containing 10% FBS (600 μl). After 48-h culture at 37˚C, cells were dyed with 0.5% crystal violet for 20 min at room temperature and under the light microscope (Nikon Corporation), five fields (magnification, x200) were randomly selected, and the mean number of cells was calculated and used for statistical analysis (26).

Annexin V/PI double staining. To assess apoptosis, SKOV3 cells were stained using Annexin V and propidium iodide as part of the Annexin V-FITC/PI Apoptosis Detection kit (BD Biosciences), according to the manufacturer's protocol and early + late cell apoptosis were analyzed using flow cytometry (Cytomics FC500 MPL; Beckman Coulter, Inc.) and FACS DiVa 6.1.3 software (BD Biosciences) (27).

Reverse transcription-quantitative PCR (RT-qPCR). After RNA extraction from of OC tissue or cells using TRIzol reagent (Invitrogen; Thermo Fisher Scientific, Inc.), reverse transcription of RNA into cDNA was performed using the PrimeScript RT Master Mix kit (Takara Biotechnology Co., Ltd.) and Mir-X miRNA RT-qPCR SYBR kit (Takara

Biotechnology Co., Ltd.) based on manufacturer's instructions. qPCR was performed using SYBR Premix Ex Taq II (Takara Biotechnology Co., Ltd.) in the ABI·7500 system. The reaction conditions were as follows, pre-denaturation 95˚C for 5 min, 40 cycles: denaturation 95˚C for 5 sec, annealing 60˚C for 30 sec, and extension 74˚C for 30 sec. The $2^{-\Delta\Delta Cq}$ method was utilized to analyze the relative expression levels of genes, which was normalized to U6 or GAPDH (Table SII) (28).

Western blot assay. Total protein of OC tissue or cells was separated by radio-immunoprecipitation assay lysis buffer (Beyotime Institute of Biotechnology) that contained protease inhibitors and phenylmethanesulfonyl fluoride (Biocolor, Ltd.), and then quantified using the BCA Protein Assay Kit (Beyotime Institute of Biotechnology). Proteins (25 μg/lane) were separated by 10% SDS-PAGE, transferred to a PVDF membrane (Bio-Rad), blocked in 5% skim milk for 1 h at room temperature, mixed overnight at 4˚C with primary antibodies against DDX5 (1:1,000; cat. no. ab128928), CD9 (1:1,000; cat. no. ab236630), CD81 (1:2,000; cat. no. ab109201) and GAPDH (1:2,500; cat. no. ab181602) and cultured for 1 h at room temperature with goat anti-rabbit IgG (1:2,000; cat. no. ab6721) (all from Abcam). Visualization of protein bands was performed in a gel imaging system (G:BOXChemi XR5; Syngene Europe), and the data analyzed using the ImageJ software (version 1.8.0; National Institutes of Health) (29).

Bioinformatical analysis and dual luciferase reporter gene assay. The targets of miR-125b-5p were predicted using bioinformatical analysis via the online ENCORI database (version 3.0; https://rnasysu.com/encori/). Subsequently, DDX5 was selected, and the relationship was analyzed using a dual luciferase reporter gene assay. The sequence containing the miR-125b-5p binding site in the DDX5 3'UTR was amplified and cloned into the pGL3-basic luciferase plasmid (Takara Biotechnology Co., Ltd.) to construct a recombinant plasmid of wild-type DDX5 (DDX5-WT; point mutation, 5'-UCAGGG-3'). Mutant DDX5 (DDX5-Mut; point mutation, 5'-ACCCCC-3') recombinant plasmid was constructed by mutating the miR-125b-5p binding site on DDX5-WT using a point mutation kit (Takara Biotechnology Co., Ltd.). Plasmid design and construction was performed by Takara Biotechnology Co., Ltd.). After 48 h transfection with the recombinant vector and miR-125b-5p mimic or mimic NC by using Lipofectamine® 3000 (Invitrogen; Thermo Fisher Scientific, Inc.), the luciferase activity of SKOV3 cells was examined using the Dual Luciferase Reporter Assay System (Promega Corporation) according to the manufacturer's instructions. Relative firefly luciferase activity was normalized to *Renilla* luciferase activity as a control for transfection efficiency (30).

RNA immunoprecipitation (RIP) assay. In accordance with the manufacturer's instructions, the binding of miR-125b-5p to DDX5 was analyzed using the Magna RIP RNA-Binding Protein Immunoprecipitation Kit (MilliporeSigma). Cells in logarithmic growth period were harvested and lysed in 500 μl RIP lysis buffer containing protease inhibitor cocktail and RNA inhibitor (included in the kit). The supernatant was collected by centrifugation at 5,000 x g for 10 min at 4˚C. The supernatant was incubated with 900 μl RIP buffer containing 5 μg of Ago2 antibody (cat. no. ab186733; Abcam) or negative control anti-IgG (cat. no. ab172730; Abcam) beads overnight at 4˚C. After washing with 500 μl washing buffer, the immunoprecipitated RNA was isolated with TRIzol reagent. RT-qPCR was performed as aforementioned with the immunoprecipitated RNA (31-33).

Statistical analysis. Data were statistically analyzed using the SPSS software (version 21.0; IBM Corp.) and expressed as mean ± standard deviation. Comparison between two groups was performed using an unpaired independent samples t-test, while comparisons among multiple groups were conducted using one-way ANOVA followed by Tukey's post hoc test. Pearson's correlation test was utilized to assess correlation. $P<0.05$ was considered to indicate a statistically significant difference. All experiments were repeated 3 times.

Results

Identification of BMSCs and exosomes. BMSCs were identified using flow cytometry, which showed that BMSCs were positive for CD29, CD44 and CD90, and negative for CD45 (Fig. 1A). BMSCs were subjected to lipogenic and osteogenic differentiation experiments (Fig. 1B). After Oil Red O staining, red lipid droplets were observed in the cells. Following Alizarin Red staining, BMSCs appeared cubic and had aggregated to form mineralized nodules, further indicating that the isolated cells were BMSCs.

TEM images demonstrated that isolated vesicles had an elliptical shape (Fig. 1C). The NTA results suggested that the vesicles diameter ranged from 30 to 200 nm (Fig. 1D). Western blotting demonstrated that the vesicles expressed CD81 and CD9 (Fig. 1E), indicating that the isolated vesicles were exosomes (34).

To evaluate if BMSCs-Exo could be used as effective vehicles for miR-125b-5p delivery to suppress OC cells proliferation and invasion, BMSCs were subject to miR-125b-5p mimic transfection, and significantly increased miR-125b-5p expression levels in BMSCs were demonstrated using RT-qPCR (Fig. 1F). PKH26-labeled exosomes were incubated with SKOV3 cells, and fluorescence microscopy demonstrated red fluorescence of PKH26 in SKOV3 cells after co-culture (Fig. 1G). miR-125b-5p mimic and mimic NC were transfected into BMSCs, post-transfected cell culture medium was obtained, and Exos were extracted from the supernatant of the medium. RT-qPCR was performed to evaluate miR-125b-5p expression levels in the extracted exosomes, and it was demonstrated (Fig. 1H) that miR-125b-5p expression levels were significantly increased in Exo-miR-125b-5p mimic group compared with that in the Exo-mimic NC group.

BMSCs-Exo limits OC cell malignancy. MSCs can inhibit the development of SKOV3 cells (35). miR-125b-5p expression levels in SKOV3 cells after co-culture with BMSCs-Exo were examined. BMSCs-Exo treatment resulted in significantly increased miR-125b-5p expression levels in SKOV3 cells (Fig. 2A). The CCK-8 (Fig. 2B), scratch (Fig. 2C) and

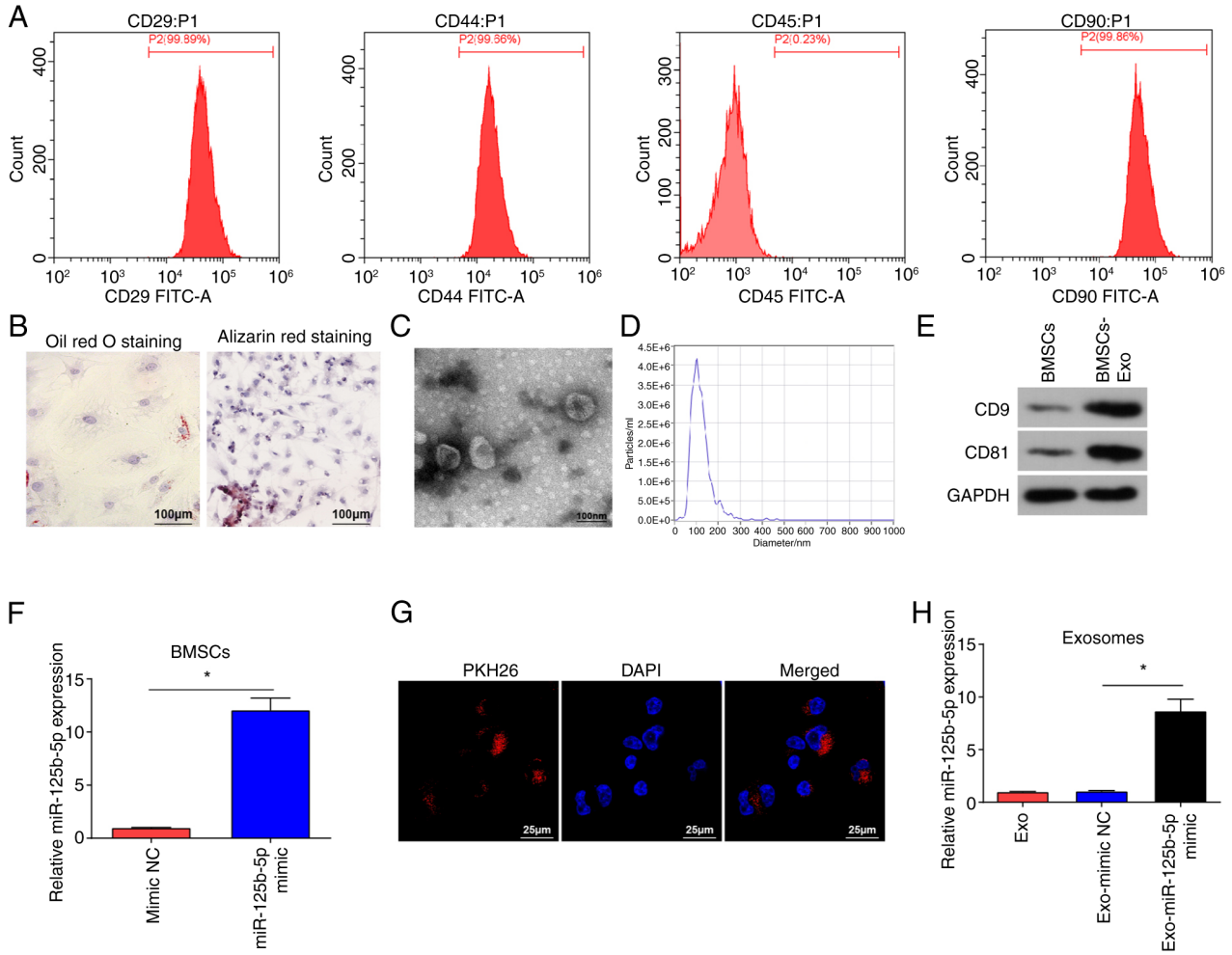

Figure 1. Identification of BMSCs and exosomes. (A) Stem cell markers detected using flow cytometry. (B) Oil Red O and Alizarin Red staining of BMSCs. Scale bar, 100 μm. (C) Representative transmission electron microscopy images of exosomes. Scale bar, 100 nm. (D) Nanoparticle tracking analysis detected the diameter and concentration of exosomes. (E) Western blot analysis of the exosomal markers, CD9 and CD81, with GAPDH as a loading controls. (F) The gene expression levels of miR-125b-5p in BMSCs transfected with miR-125b-5p mimic. (G) PKH26-labeled exosomes in SKOV3 cells. Scale bar, 25 μm. (H) miR-125b-5p gene expression levels in Exo-miR-125b-5p mimic and Exo-mimic were assessed. Data were represented by the mean ± standard deviation. *P<0.05. BMSCs, bone mesenchymal stem cells; miR-125b-5p, microRNA-125b-5p; NC, negative control; Exo-, exosome encapsulated.

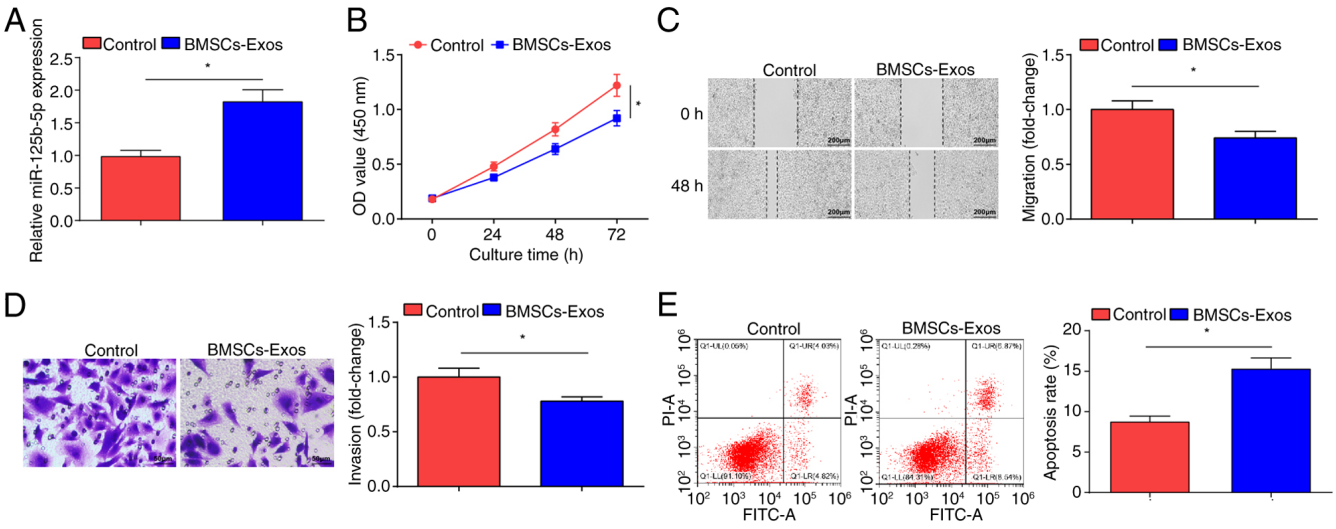

Figure 2. BMSCs-Exo limits malignancy of OC cells. (A) miR-125b-5p gene expression levels evaluated in SKOV3 cells treated with BMSCs-Exo. (B) Proliferation of OC cells examined using the CCK-8 assay after BMSCs-Exo treatment. (C) Migration of OC cells assessed using a scratch test after BMSCs-Exo treatment (scale bar, 200 μm; magnification, x100). (D) Invasion of OC cells evaluated using a Transwell assay after BMSCs-Exo treatment (scale bar, 50 μm; magnification, x200). (E) Apoptosis of OC cells examined using flow cytometry after BMSCs-Exo treatment. Data were represented by the mean ± standard deviation. *P<0.05. BMSCs-Exo, bone mesenchymal stem cells-derived exosomes; OC, ovarian cancer; OD, optical density.

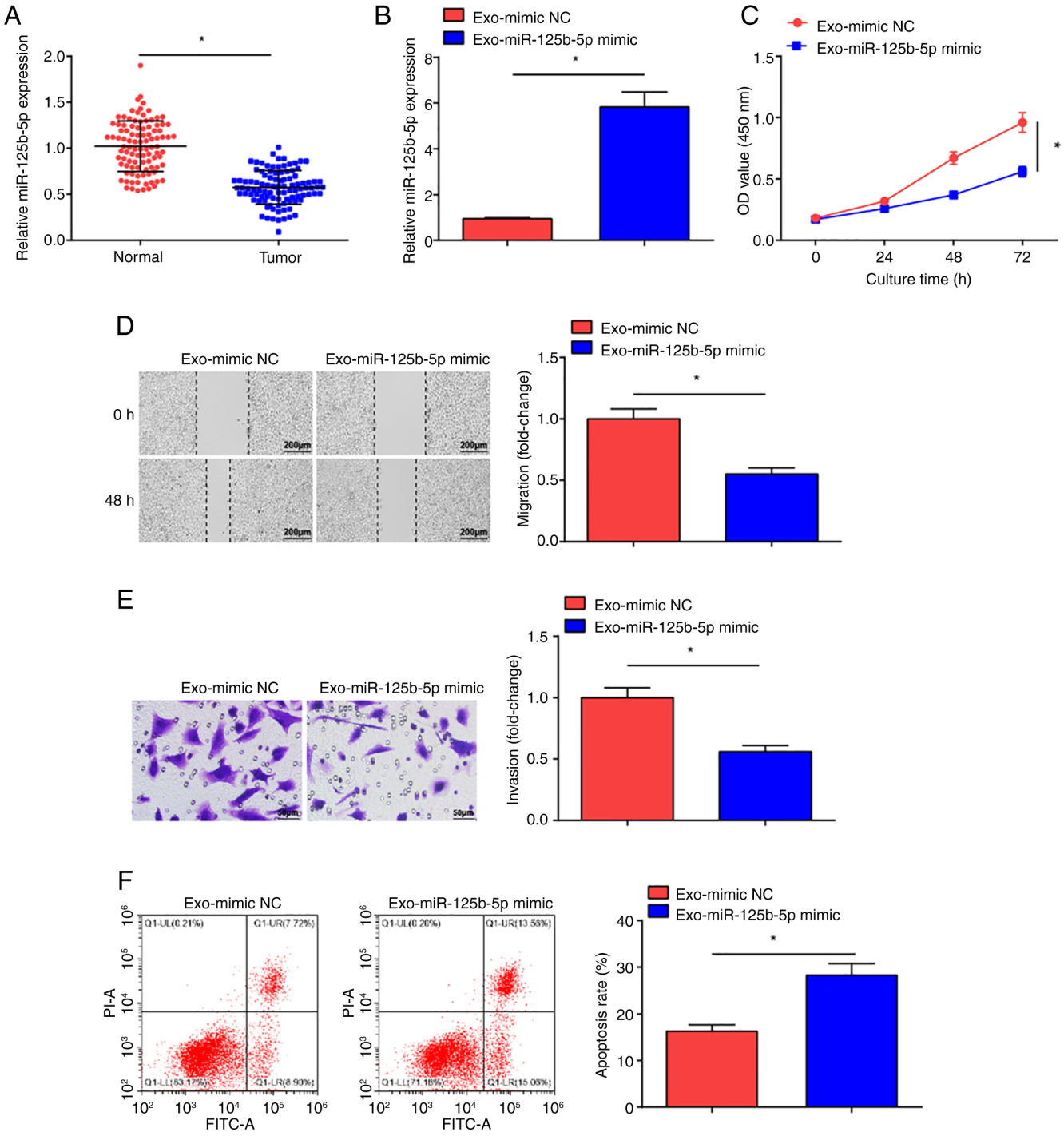

Figure 3. Exosome delivery of miR-125b-5p represses malignant progression of OC cells. (A) Gene expression levels of miR-125b-5p in normal ovarian tissues and OC tissues detected. (B) miR-125b-5p gene expression levels in SKOV3 cells treated with Exo-miR-125b-5p mimic and Exo-mimic NC. (C) Proliferation of OC cells examined using the CCK-8 assay after Exo-miR-125b-5p mimic treatment. (D) Migration of OC cells evaluated using a scratch test after Exo-miR-125b-5p mimic treatment (scale bar, 200 μm; magnification, x100). (E) Invasion of OC cells assessed using a Transwell assay after Exo-miR-125b-5p mimic treatment (scale bar, 50 μm; magnification, x200). (F) Apoptosis of OC cells examined using flow cytometry after Exo-miR-125b-5p mimic treatment. Data were represented by the mean ± standard deviation. *P<0.05. OC, ovarian cancer; OD, optical density; miR-125b-5p, microRNA-125b-5p; NC, negative control; Exo-, exosome encapsulated.

Transwell (Fig. 2D) assays demonstrated that treatment with BMSCs-Exo significantly impaired the proliferation, migration and invasion of SKOV3 cells compared with the control cells; however, flow cytometry demonstrated that the apoptotic rate of the BMSCs-Exo treated cells significantly increased (Fig. 2E). Overall, BMSCs-Exo inhibited the development of OC cells *in vitro*.

Exosome mediated delivery of miR-125b-5p represses malignant progression of OC cells. miR-125b-5p can inhibit cancer cell malignancy (36). Significantly decreased miR-125b-5p expression levels were measured in the tumor tissue samples from patients with OC compared with normal tissue samples (Fig. 3A). To determine whether BMSCs-Exo carrying miR-125b-5p could impact OC cell development, the exosomes

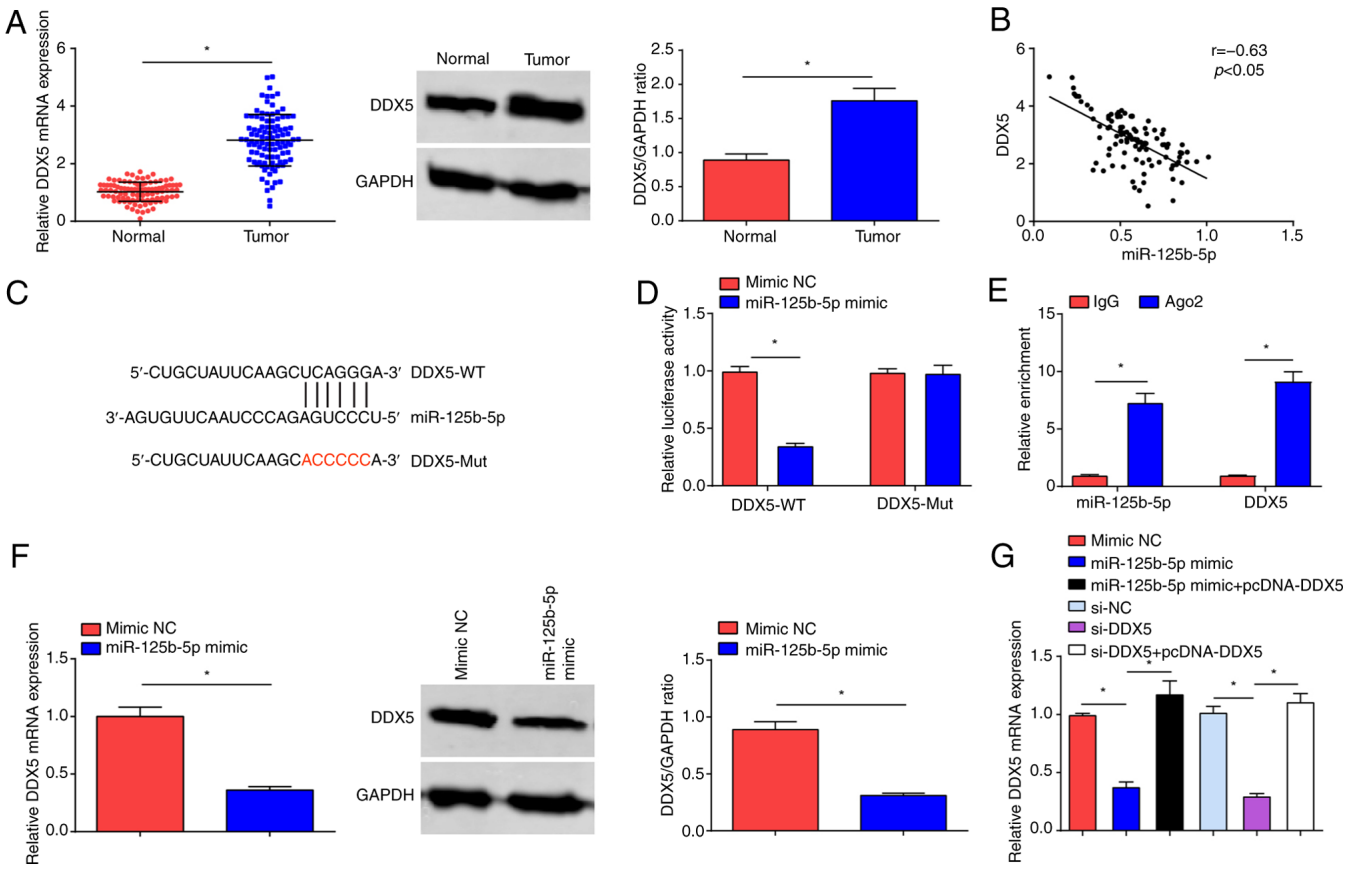

Figure 4. Targeting relationship between miR-125b-5p and DDX5. (A) DDX5 mRNA and protein expression in normal ovarian and tumor tissues. (B) Targeted sites between miR-125b-5p and DDX5 using the ENCORI software. (C) Correlation between miR-125b-5p and DDX5 mRNA expression levels. The binding of miR-125b-5p and DDX5 was analyzed using (D) dual luciferase reporter and (E) RNA immunoprecipitation assays. (F) DDX5 mRNA and protein expression levels were evaluated in mimic NC and miR-125b-5p mimic group. (G) DDX5 mRNA expression levels were evaluated. Data were represented by the mean ± standard deviation. *P<0.05. OC, ovarian cancer; OD, optical density; miR-125b-5p, microRNA-125b-5p; NC, negative control; Exo-, exosome encapsulated; WT, wild-type; Mut, mutant; DDX, DEAD-box helicase 5.

Exo-miR-125b-5p mimic and Exo-mimic NC were co-cultured with SKOV3 cells, and miR-125b-5p expression levels in SKOV3 cells were evaluated (Fig. 3B). Significantly increased expression levels of miR-125b-5p were observed in the Exo-miR-125b-5p mimic-treated SKOV3 cells compared with the Exo-mimic NC treatment. The CCK-8 assay (Fig. 3C), scratch (Fig. 3D) and Transwell (Fig. 3E) assays, and flow cytometry (Fig. 3F) demonstrated that the proliferative, migratory and invasive properties of Exo-miR-125b-5p mimic-treated SKOV3 cells were significantly reduced and apoptosis was significantly increased in comparison with Exo-mimic NC treatment. These results suggest that miR-125b-5p delivered by BMSCs-Exo impeded OC development.

Targeting relationship between miR-125b-5p and DDX5. RT-qPCR and western blot assays demonstrated that DDX5 expression was significantly increased in OC tumor tissues compared with normal tissue (Fig. 4A). To confirm the regulatory relationship between miR-125b-5p and DDX5, bioinformatics analysis software predicted the binding sites between them (Fig. 4B), and Pearson's correlation test demonstrated significant negative correlation between the mRNA expression levels of miR-125b-5p and DDX5 (Fig. 4C). Furthermore, miR-125b-5p mimic inhibited the luciferase activity of DDX5-WT, while had no impact on the luciferase activity of DDX5-Mut (Fig. 4D). The RIP experiment demonstrated that miR-125b-5p and DDX5 expression levels were significantly increased with Ago2 treatment (Fig. 4E). RT-qPCR and western blot analysis indicated that DDX5 expression levels were significantly reduced upon miR-125b-5p overexpression (Fig. 4F). RT-qPCR also demonstrated that overexpression of DDX5 reversed the suppressive effect of either miR-125b-5p mimic or si-DDK5 on DDK5 expression levels (Fig. 4G).

DDX5 knockdown inhibits the malignant progression of OC cells. si-NC and si-DDX5 were introduced into SKOV3 cells; si-DDX5 transfection inhibited DDX5 expression levels in SKOV3 cells (Fig. 5A and B). The CCK-8 (Fig. 5C), scratch (Fig. 5D) and Transwell (Fig. 5E) assays, and flow cytometry (Fig. 5F) demonstrated that following the inhibition of DDX5 expression, the proliferative, migratory and invasive properties of OC cells were significantly reduced, and cell apoptosis was significantly increased in the si-DDX5 group compared with that in the si-NC group. In brief, DDX5 suppression inhibited OC cell progression.

DDX5 overexpression abrogates miR-125b-5p-induced suppression of OC development. To verify that BMSCs-Exo carrying miR-125b-5p targeting DDX5 can regulate OC

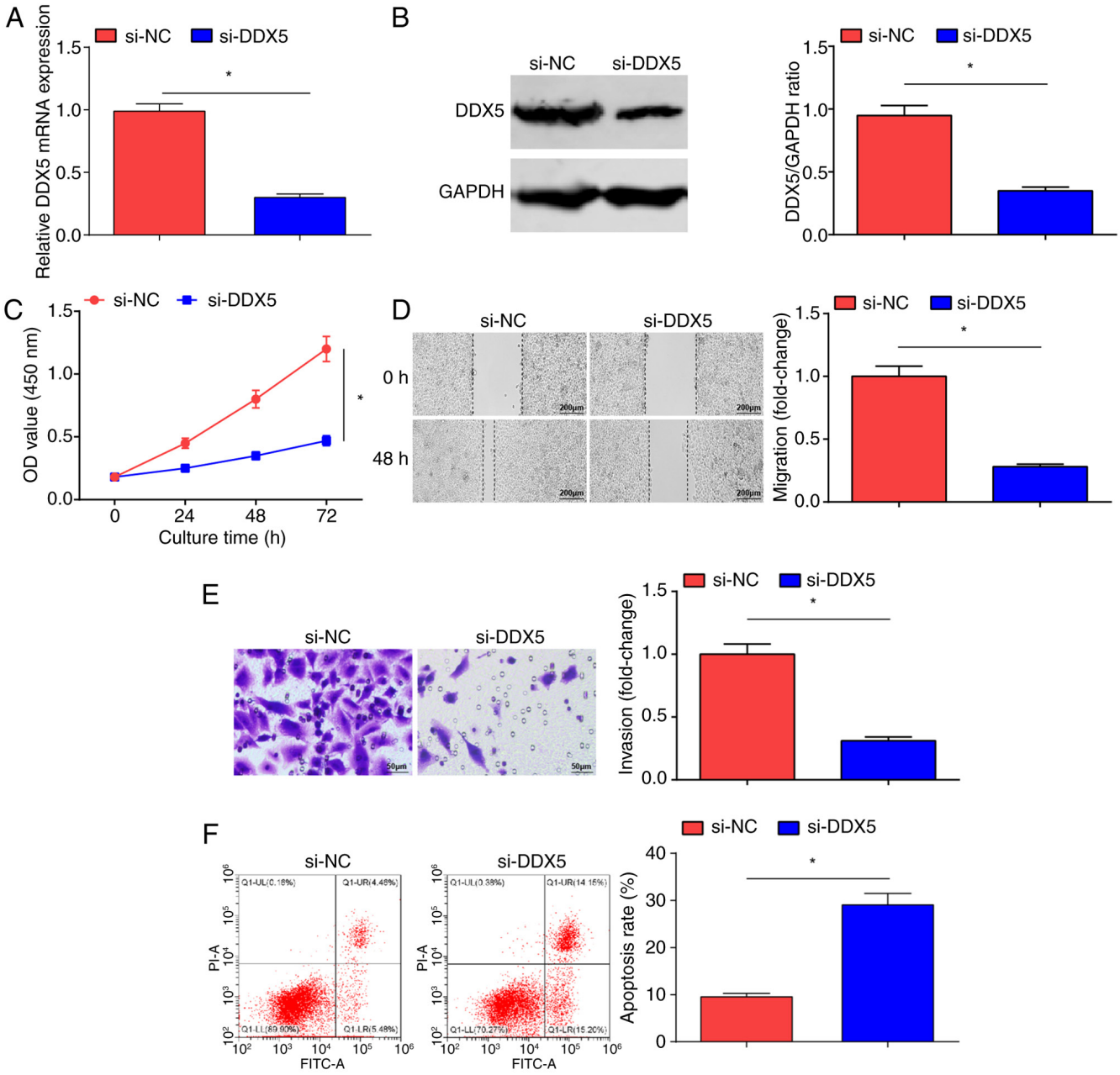

Figure 5. DDX5 knockdown inhibited the malignancy of OC cells. DDX5 (A) mRNA and (B) protein expression levels upon transfection of si-DDX5. (C) Proliferation of OC cells evaluated by CCK-8 assay upon transfection of si-DDX5. (D) Migration of OC cells assessed using a scratch test upon transfection of si-DDX5 (Scale bar, 200 μm; magnification, x100). (E) Invasion of OC cells tested using a Transwell assay upon transfection of si-DDX5 (scale bar, 50 μm; magnification, x200). (F) Apoptosis of OC cells evaluated using flow cytometry upon transfection of si-DDX5. Data were represented by the mean ± standard deviation. *P<0.05. OC, ovarian cancer; OD, optical density; NC, negative control; DDX, DEAD-box helicase 5; si, small interfering.

development, pcDNA-NC and pcDNA-DDX5 were transfected into SKOV3 cells. RT-qPCR experiments showed that the expression levels of DDX5 mRNA were significantly elevated in the pcDNA-DDX5 group compared with the pcDNA-NC group (Fig. 6A). Next, the Exo-miR-125b-5p mimic + pcDNA-NC group and the Exo-miR-125b-5p mimic + pcDNA-DDX5 group were examined. Significantly increased DDX5 expression levels were observed in the Exo-miR-125b-5p mimic + pcDNA-DDX5 group compared with the Exo-miR-125b-5p mimic + pcDNA-NC group (Fig. 6B and C). The CCK-8, (Fig. 6D) scratch (Fig. 6E) and Transwell (Fig. 6F) assays, and flow cytometry (Fig. 6G) demonstrated that the proliferative, migratory and invasive properties of OC cells were significantly increased, and that cell apoptosis was significantly reduced in the Exo-miR-125b-5p mimic + pcDNA-DDX5 group compared with the Exo-miR-125b-5p mimic + pcDNA-NC group. In summary, miR-125b-5p, derived from BMSCs-Exo, served a key role in inhibiting OC cell growth by targeting DDX5.

Discussion

OC is the deadliest gynecological malignancy worldwide that is often diagnosed at advanced stages with poor outcomes (37). Focusing on the biological functions of OC cells, the present study demonstrated that BMSCs-Exo delivery of miR-125b-5p

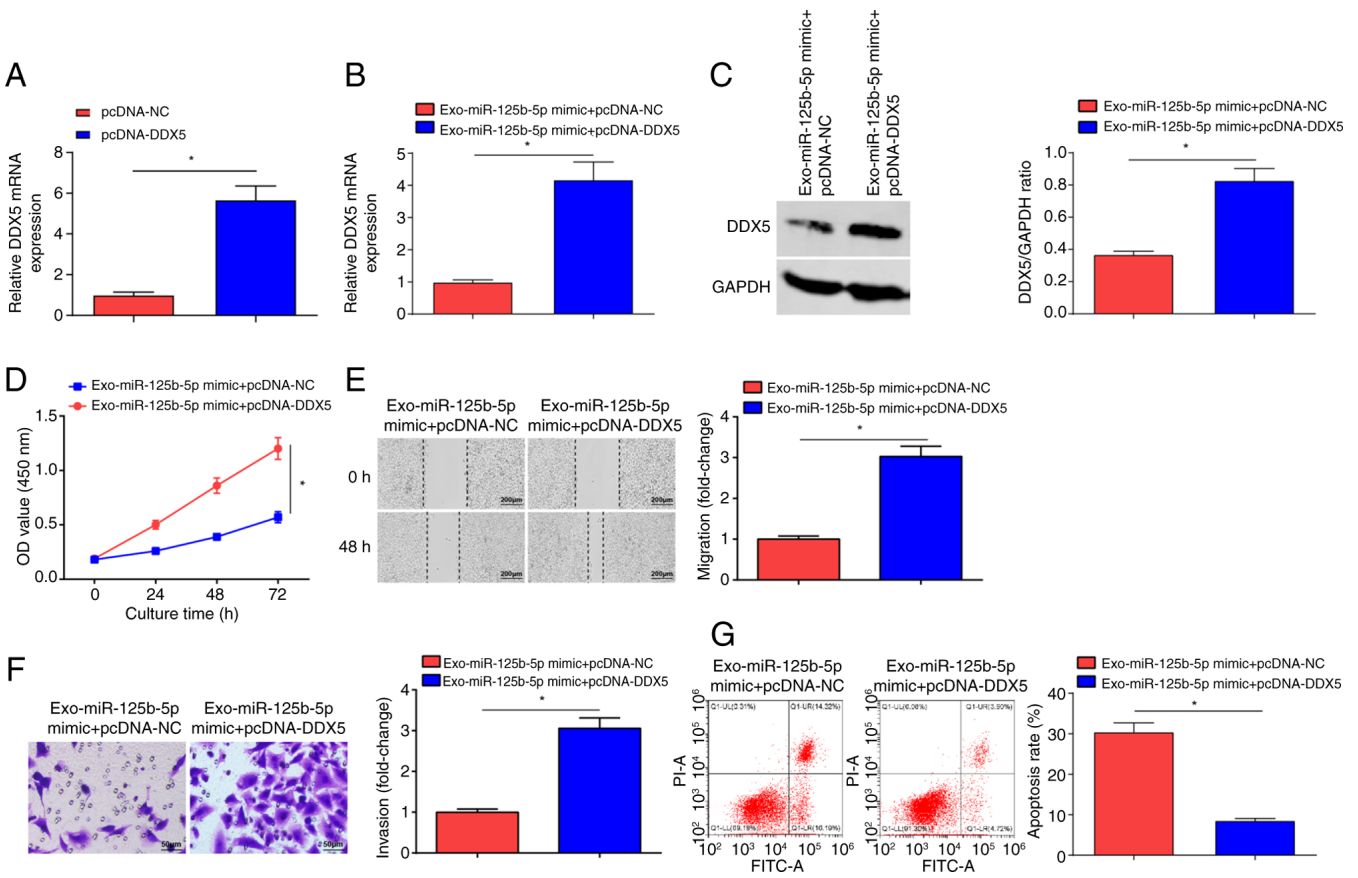

Figure 6. DDX5 overexpression inhibits miR-125b-5p-induced suppression of OC development. (A) DDX5 mRNA expression in the pcDNA-NC group and pcDNA-DDX5 group. DDX5 (B) mRNA and (C) protein expression levels in the Exo-miR-125b-5p mimic + pcDNA-NC and Exo-miR-125b-5p mimic + pcDNA-DDX5 groups. (D) Proliferation of OC cells examined using the CCK-8 assay in the Exo-miR-125b-5p mimic + pcDNA-NC and Exo-miR-125b-5p mimic + pcDNA-DDX5 groups. (E) Migration of OC cells evaluated using a scratch test in the Exo-miR-125b-5p mimic + pcDNA-NC and Exo-miR-125b-5p mimic + pcDNA-DDX5 groups (scale bar, 200 μm; magnification, x100). (F) Invasion of OC cells assessed using a Transwell assay in the Exo-miR-125b-5p mimic + pcDNA-NC and Exo-miR-125b-5p mimic + pcDNA-DDX5 groups (scale bar, 50 μm; magnification, x200). (G) Apoptosis of OC cells examined using flow cytometry in the Exo-miR-125b-5p mimic + pcDNA-NC and Exo-miR-125b-5p mimic + pcDNA-DDX5 groups. Data were represented by the mean ± standard deviation. *P<0.05. OC, ovarian cancer; OD, optical density; miR-125b-5p, microRNA-125b-5p; NC, negative control; Exo-, exosome encapsulated; WT, wild-type; Mut, mutant; DDX, DEAD-box helicase 5; transfected using the pcDNA3.1 plasmid.

had anti-tumorigenic effects in OC cells via direct targeting of DDX5.

BMSCs-Exo co-culture reduced proliferation, invasion, migration and elevated apoptosis of OC cells *in vitro*. A previous study by Qiu *et al* (9) reported MSC-Exo-mediated effects on reducing cell growth in OC. The combination of MSC-Exo and radiotherapy has a regulatory role in the control of enhanced radiation effects on metastasis and the spread of melanoma cells (38). Furthermore, an observation by Xu *et al* (39) demonstrated that glioma cells treated with MSCs-Exo show reduced proliferation, invasion and migration. Shang *et al* (40) reported the tumor-suppressor effects of MSCs-Exo delivering high levels of miR-1231 on the proliferation, migration and invasion of pancreatic cancer cells. Furthermore, a previous study suggested human umbilical cord MSCs-Exo as a feasible therapeutic strategy in the control of outgrowth of esophageal squamous cell carcinoma cells *in vitro* and *in vivo* through transfer of miR-375 (41). Briefly, MSCs-Exo themselves have anti-tumorigenic effects and their delivery of targeted nucleic acids also contributes to cancer control.

Expression levels of miR-125b-5p were significantly reduced in tumor tissue samples of patients with OC. miR-125b-5p downregulation has been demonstrated in several types of cancer, including EOC (13) and colon cancer (42). In regards to the delivery capacity of BMSCs-Exo, miR-125b-5p was transported into SKOV3 cells, so as to lower the malignant abilities of cells *in vitro*. Liu *et al* (43) have reported that in bladder cancer cells, upon overexpressing miR-125b-5p, cell viability and migration are inhibited, whereas apoptosis is induced. By contrast, overexpression of miR-125b-5p has been reported to have a role in impairing the proliferative, migratory and invasive properties of breast cancer cells (44). In the presence of cisplatin, overexpression of miR-125b-5p in gallbladder cancer cells increases apoptosis levels and decreases tumor formation, but inhibition of miR-125b-5p decreases apoptosis levels and increases tumor formation (45). It was reported that in hepatocellular carcinoma, miR-125b-5p overexpression limits the malignant phenotype of tumor cells (36). In the development of esophageal squamous cell carcinoma cells, overexpression of miR-125b-5p can induce cell senescence and also slow down the process of epithelial to mesenchymal transition (46). Overall, in numerous types of cancer, including OC, miR-125b-5p exerts protective effects to slow down malignant progression.

DDX5 was upregulated in OC, and DDX5 silencing led to the blockade of OC cell outgrowth *in vitro*. Similar to the present findings, Zhang *et al* (47) also reported high expression levels of DDX5 in colorectal cancer. DDX5 is upregulated in small cell lung cancer and its inhibition results in reduced growth of tumor cells resistant to chemotherapy (48). DDX5 is upregulated in gastric cancer, and inhibition of DDX5 inhibits growth of cells and xenografts, whereas overexpression of DDX5 promotes cell proliferation, migration and invasion (17). Also, DDX5 was identified as a target involved in miR-125b-5p-mediated OC cell growth, as DDX5 overexpression caused the reversal of upregulated miR-125b-5p-induced repression of OC cell development. Mechanistically, high expression levels of DDX5 can re-activate carcinogenesis of endometrial cancer cells mediated by silenced hepatoma-derived growth factor (49). Furthermore, Wang *et al* (50) demonstrated that DDX5 overexpression increases the proliferation of non-small-cell lung cancer cells *in vitro* and *in vivo*. Collectively, modification of DDX5 expression represents a switch in the progression of tumors.

In the present study, a binding site between miR-125b-5p and DDX5 was identified by confirming the regulatory relationship between miR-125b-5p and DDX5 and demonstrating that miR-125b-5p was negatively correlated with DDX5. Following this, a binding site between miR-125b-5p and DDX5 was experimentally demonstrated by online database, indicating that miR-125b-5p had a role in regulating DDX5 expression. In addition, downregulation of DDX5 expression levels could inhibit the proliferation and malignant progression of OC cells. It was hypothesized that there was a targeting relationship between miR-125b-5p and DDX5 expression in OC cells derived from exosomes of bone marrow MSCs. The experimental results were as hypothesized, as the Exo + miR-125b-5p + pcDNA-DDX5 group demonstrated increased cell viability, migratory and invasive ability, and decreased apoptosis rate in OC cells. DDX5 overexpression reversed the effects of MSC-derived Exo miR-125b-5p on OC cell proliferation and invasion, while bone marrow MSC-derived Exo miR-125b-5p inhibited OC cell proliferation and tumor progression by targeting DDX5. In the future, we will conduct further validation of the related downstream mechanisms.

In summary, miR-125b-5p delivered by BMSCs-Exo could inhibit OC progression, which was associated with DDX5 downregulation. The present study advances the understanding of existing molecular mechanisms in OC, and explores the feasibility of drug delivery using BMSCs-Exo.

Acknowledgements

Not applicable.

Funding

No funding was received.

Availability of data and materials

The data generated in the present study may be requested from the corresponding author.

Authors' contributions

YW and WW contributed to conception and design of manuscript and manuscript editing. DZ contributed to revising the manuscript critically for important intellectual content and experimental studies. YG contributed to analysis and interpretation of data. WW and YW confirmed the authenticity of all the raw data. All authors read and approved the final version of the manuscript.

Ethics approval and consent to participate

Experiments were performed after approval by the Ethics Committee of Harbin Medical University Cancer Hospital (approval no. 20200316; Harbin, China), and written informed consent was provided by each patient. BMSCs were used in accordance with the International Society for Stem Cells Research guidelines for Stem Cell Research and Clinical Translation and approved by the Ethics Committee of Harbin Medical University Cancer Hospital (approval no. 20200518).

Patient consent for publication

Not applicable.

Competing interests

The authors declare that they have no competing interests.

References

1. Sung H, Ferlay J, Siegel RL, Laversanne M, Soerjomataram I, Jemal A and Bray F: Global cancer statistics 2020: GLOBOCAN estimates of incidence and mortality worldwide for 36 cancers in 185 countries. CA Cancer J Clin 71: 209-249, 2021.
2. Stewart C, Ralyea C and Lockwood S: Ovarian cancer: An integrated review. Semin Oncol Nurs 35: 151-156, 2019.
3. Rooth C: Ovarian cancer: Risk factors, treatment and management. Br J Nurs 22: S23-S30, 2013.
4. Narod S: Can advanced-stage ovarian cancer be cured? Nat Rev Clin Oncol 13: 255-261, 2016.
5. Crapnell K, Blaesius R, Hastings A, Lennon DP, Caplan AI and Bruder SP: Growth, differentiation capacity, and function of mesenchymal stem cells expanded in serum-free medium developed via combinatorial screening. Exp Cell Res 319: 1409-1418, 2013.
6. Mohr A and Zwacka R: The future of mesenchymal stem cell-based therapeutic approaches for cancer-from cells to ghosts. Cancer Lett 414: 239-249, 2018.
7. Mendt M, Rezvani K and Shpall E: Mesenchymal stem cell-derived exosomes for clinical use. Bone Marrow Transplant 54 (Suppl 2): S789-S792, 2019.
8. Tan F, Li X, Wang Z, Li J, Shahzad K and Zheng J: Clinical applications of stem cell-derived exosomes. Signal Transduct Target Ther 9: 17, 2024.
9. Qiu L, Wang J, Chen M, Chen F and Tu W: Exosomal microRNA-146a derived from mesenchymal stem cells increases the sensitivity of ovarian cancer cells to docetaxel and taxane via a LAMC2-mediated PI3K/Akt axis. Int J Mol Med 46: 609-620, 2020.
10. Ono M, Kosaka N, Tominaga N, Yoshioka Y, Takeshita F, Takahashi RU, Yoshida M, Tsuda H, Tamura K and Ochiya T: Exosomes from bone marrow mesenchymal stem cells contain a microRNA that promotes dormancy in metastatic breast cancer cells. Sci Signal 7: ra63, 2014.
11. Jiang S, Mo C, Guo S, Zhuang J, Huang B and Mao X: Human bone marrow mesenchymal stem cells-derived microRNA-205-containing exosomes impede the progression of prostate cancer through suppression of RHPN2. J Exp Clin Cancer Res 38: 495, 2019.

12. Kalinkova L, Kajo K, Karhanek M, Wachsmannova L, Suran P, Zmetakova I and Fridrichova I: Discriminating miRNA profiles between endometrioid well- and poorly-differentiated tumours and endometrioid and serous subtypes of endometrial cancers. Int J Mol Sci 21: 6071, 2020.
13. de Lima AB, Silva LM, Gonçales NG, Carvalho MRS, da Silva Filho AL and da Conceição Braga L: Three-dimensional cellular arrangement in epithelial ovarian cancer cell lines TOV-21G and SKOV-3 is associated with apoptosis-related miRNA expression modulation. Cancer Microenviron 11: 85-92, 2018.
14. Liu J, Zhang X, Huang Y, Zhang Q, Zhou J, Zhang X and Wang X: miR-200b and miR-200c co-contribute to the cisplatin sensitivity of ovarian cancer cells by targeting DNA methyltransferases. Oncol Lett 17: 1453-1460, 2019.
15. Xing Z, Ma WK and Tran EJ: The DDX5/Dbp2 subfamily of DEAD-box RNA helicases. Wiley Interdiscip Rev RNA 10: e1519, 2019.
16. Li Z, Caron de Fromentel C, Kim W, Wang WH, Sun J, Yan B, Utturkar S, Lanman NA, Elzey BD, Yeo Y, *et al*: RNA helicase DDX5 modulates sorafenib sensitivity in hepatocellular carcinoma via the Wnt/β-catenin-ferroptosis axis. Cell Death Dis 14: 786, 2023.
17. Du C, Li DQ, Li N, Chen L, Li SS, Yang Y, Hou MX, Xie MJ and Zheng ZD: DDX5 promotes gastric cancer cell proliferation in vitro and in vivo through mTOR signaling pathway. Sci Rep 7: 42876, 2017.
18. Ye X: Confluence analysis of multiple omics on platinum resistance of ovarian cancer. Eur J Gynaecol Oncol 36: 514-519, 2015.
19. Xu CM, Chen LX, Gao F, Zhu MF, Dai Y, Xu Y and Qian WX: MiR-431 suppresses proliferation and metastasis of lung cancer via down-regulating DDX5. Eur Rev Med Pharmacol Sci 23: 699-707, 2019.
20. Mallmann-Gottschalk N, Sax Y, Kimmig R, Lang S and Brandau S: EGFR-specific tyrosine kinase inhibitor modifies NK cell-mediated antitumoral activity against ovarian cancer cells. Int J Mol Sci 20: 4693, 2019.
21. Mahmoudian-Sani MR, Forouzanfar F, Asgharzade S and Ghorbani N: Overexpression of MiR-183/96/182 triggers retina-like fate in human bone marrow-derived mesenchymal stem cells (hBMSCs) in culture. J Ophthalmol 2019: 2454362, 2019.
22. Li B, Luan S, Chen J, Zhou Y, Wang T, Li Z, Fu Y, Zhai A and Bi C: The MSC-derived exosomal lncRNA H19 promotes wound healing in diabetic foot ulcers by upregulating PTEN via MicroRNA-152-3p. Mol Ther Nucleic Acids 19: 814-826, 2020.
23. Li W, Han Y, Zhao Z, Ji X, Wang X, Jin J, Wang Q, Guo X, Cheng Z, Lu M, *et al*: Oral mucosal mesenchymal stem cell-derived exosomes: A potential therapeutic target in oral premalignant lesions. Int J Oncol 54: 1567-1578, 2019.
24. Sun P, Fan X, Hu X, Fu X, Wei Q and Zang Y: circPCNX and pecanex promote hepatocellular carcinoma cell viability by inhibiting miR-506. Cancer Manag Res 11: 10957-10967, 2019.
25. Jiang F, Chen Y, Ren S, Li Z, Sun K, Xing Y, Zhu Y and Piao D: Cyclovirobuxine D inhibits colorectal cancer tumorigenesis via the CTHRC1-AKT/ERK-Snail signaling pathway. Int J Oncol 57: 183-196, 2020.
26. Wang S, Su X, Xu M, Xiao X, Li X, Li H, Keating A and Zhao RC: Exosomes secreted by mesenchymal stromal/stem cell-derived adipocytes promote breast cancer cell growth via activation of Hippo signaling pathway. Stem Cell Res Ther 10: 117, 2019.
27. Sun H, Wang H, Wang X, Aoki Y, Wang X, Yang Y, Cheng X, Wang Z and Wang X: Aurora-A/SOX8/FOXK1 signaling axis promotes chemoresistance via suppression of cell senescence and induction of glucose metabolism in ovarian cancer organoids and cells. Theranostics 10: 6928-6945, 2020.
28. Wu X, Zhao J, Ruan Y, Sun L, Xu C and Jiang H: Sialyltransferase ST3GAL1 promotes cell migration, invasion, and TGF-β1-induced EMT and confers paclitaxel resistance in ovarian cancer. Cell Death Dis 9: 1102, 2018.
29. Wang Z, Wang P, Cao L, Li F, Duan S, Yuan G, Xiao L, Guo L, Yin H, Xie D, *et al*: Long intergenic non-coding RNA 01121 promotes breast cancer cell proliferation, migration, and invasion via the miR-150-5p/HMGA2 axis. Cancer Manag Res 11: 10859-10870, 2019.
30. Li N, Cui T, Guo W, Wang D and Mao L: MiR-155-5p accelerates the metastasis of cervical cancer cell via targeting TP53INP1. Onco Targets Ther 12: 3181-3196, 2019.
31. Liu SC, Cao YH, Chen LB, Kang R, Huang ZX and Lu XS: BMSC-derived exosomal lncRNA PTENP1 suppresses the malignant phenotypes of bladder cancer by upregulating SCARA5 expression. Cancer Biol Ther 23: 1-13, 2022.
32. Xiu C, Zheng H, Jiang M, Li J, Zhou Y, Mu L and Liu W: MSCs-derived miR-150-5p-expressing exosomes promote skin wound healing by activating PI3K/AKT pathway through PTEN. Int J Stem Cells 15: 359-371, 2022.
33. Furuta T, Miyaki S, Ishitobi H, Ogura T, Kato Y, Kamei N, Miyado K, Higashi Y and Ochi M: Mesenchymal stem cell-derived exosomes promote fracture healing in a mouse model. Stem Cells Transl Med 5: 1620-1630, 2016.
34. Zhang S, Ma Y, Hu X, Zheng Y and Chen X: Targeting PRMT5/Akt signalling axis prevents human lung cancer cell growth. J Cell Mol Med 23: 1333-1342, 2019.
35. Reza AMMT, Choi YJ, Yasuda H and Kim JH: Human adipose mesenchymal stem cell-derived exosomal-miRNAs are critical factors for inducing anti-proliferation signalling to A2780 and SKOV-3 ovarian cancer cells. Sci Rep 6: 38498, 2016.
36. Hua S, Quan Y, Zhan M, Liao H, Li Y and Lu L: miR-125b-5p inhibits cell proliferation, migration, and invasion in hepatocellular carcinoma via targeting TXNRD1. Cancer Cell Int 19: 203, 2019.
37. Wieser V, Tsibulak I, Reimer DU, Zeimet AG, Fiegl H, Hackl H and Marth C: An angiogenic tumor phenotype predicts poor prognosis in ovarian cancer. Gynecol Oncol 170: 290-299, 2023.
38. de Araujo Farias V, O'Valle F, Serrano-Saenz S, Anderson P, Andrés E, López-Peñalver J, Tovar I, Nieto A, Santos A, Martín F, *et al*: Exosomes derived from mesenchymal stem cells enhance radiotherapy-induced cell death in tumor and metastatic tumor foci. Mol Cancer 17: 122, 2018.
39. Xu H, Zhao G, Zhang Y, Jiang H, Wang W, Zhao D, Hong J, Yu H and Qi L: Mesenchymal stem cell-derived exosomal microRNA-133b suppresses glioma progression via Wnt/β-catenin signaling pathway by targeting EZH2. Stem Cell Res Ther 10: 381, 2019.
40. Shang S, Wang J, Chen S, Tian R, Zeng H, Wang L, Xia M, Zhu H and Zuo C: Exosomal miRNA-1231 derived from bone marrow mesenchymal stem cells inhibits the activity of pancreatic cancer. Cancer Med 8: 7728-7740, 2019.
41. He Z, Li W, Zheng T, Liu D and Zhao S: Human umbilical cord mesenchymal stem cells-derived exosomes deliver microRNA-375 to downregulate ENAH and thus retard esophageal squamous cell carcinoma progression. J Exp Clin Cancer Res 39: 140, 2020.
42. Shi H, Li K, Feng J, Liu G, Feng Y and Zhang X: LncRNA-DANCR interferes with miR-125b-5p/HK2 axis to desensitize colon cancer cells to cisplatin vis activating anaerobic glycolysis. Front Oncol 10: 1034, 2020.
43. Liu S, Chen Q and Wang Y: MiR-125b-5p suppresses the bladder cancer progression via targeting HK2 and suppressing PI3K/AKT pathway. Hum Cell 33: 185-194, 2020.
44. Li Y, Wang Y, Fan H, Zhang Z and Li N: miR-125b-5p inhibits breast cancer cell proliferation, migration and invasion by targeting KIAA1522. Biochem Biophys Res Commun 504: 277-282, 2018.
45. Yang D, Zhan M, Chen T, Chen W, Zhang Y, Xu S, Yan J, Huang Q and Wang J: miR-125b-5p enhances chemotherapy sensitivity to cisplatin by down-regulating Bcl2 in gallbladder cancer. Sci Rep 7: 43109, 2017.
46. Mei LL, Wang WJ, Qiu YT, Xie XF, Bai J and Shi ZZ: miR-125b-5p functions as a tumor suppressor gene partially by regulating HMGA2 in esophageal squamous cell carcinoma. PLoS One 12: e0185636, 2017.
47. Zhang M, Weng W, Zhang Q, Wu Y, Ni S, Tan C, Xu M, Sun H, Liu C, Wei P and Du X: The lncRNA NEAT1 activates Wnt/β-catenin signaling and promotes colorectal cancer progression via interacting with DDX5. J Hematol Oncol 11: 113, 2018.
48. Xing Z, Russon MP, Utturkar SM and Tran EJ: The RNA helicase DDX5 supports mitochondrial function in small cell lung cancer. J Biol Chem 295: 8988-8998, 2020.
49. Liu C, Wang L, Jiang Q, Zhang J, Zhu L, Lin L, Jiang H, Lin D, Xiao Y, Fang W and Guo S: Hepatoma-derived growth factor and DDX5 promote carcinogenesis and progression of endometrial cancer by activating β-catenin. Front Oncol 9: 211, 2019.
50. Wang Z, Luo Z, Zhou L, Li X, Jiang T and Fu E: DDX5 promotes proliferation and tumorigenesis of non-small-cell lung cancer cells by activating β-catenin signaling pathway. Cancer Sci 106: 1303-1312, 2015.